Chapter 3
Characterization Techniques for Chitosan and Its Based Nanocomposites

Gunjan Purohit and Diwan S. Rawat

Abstract Chitosan nanocomposites/nanoparticles (NPs) are biobased polymeric materials that have gained booming intent due to their versatile physicochemical characteristics and properties. The processed chitosan, i.e., chitosan nanoparticles in comparison to bulk counterparts possesses versatile biological/biodegradable applications because of their smaller sizes, higher surface area, and cationic nature. Various morphologies of chitosan are reported in the literature, viz., nano vehicles, nanoparticles, nanocomposites, fibers, meshes, nanocapsules, and so on for a variety of applications. The underlying chapter critically reviews the series of characterization techniques that determine chitosan nanocomposites' morphological and physicochemical characteristics such as surface properties, charges, particle size, particle appearance, elemental composition, and surface interactions. The current chapter is aimed to discuss the popular techniques, namely, transmission electron microscopy (TEM), scanning electron microscopy (SEM), energy-dispersive X-ray spectroscopy (EDX), X-ray photoelectron spectroscopy (XPS), X-ray diffraction (XRD), inductively coupled plasma mass spectroscopy (ICP-MS), fourier-transform infrared spectroscopy (FT-IR), atomic emission spectroscopy (AES), dynamic light scattering (DLS), atomic force microscopy (AFM), nuclear magnetic resonance (NMR), etc., which helps in determining and developing a consistent, precise, and reliable characterization of chitosan nanocomposites.

Keywords Chitosan nanoparticles · Morphological · Properties · Solid-state properties · Interaction analysis · Surface charge

Abbreviations

AAS	Atomic absorption spectroscopy
AES	Atomic emission spectroscopy
AFM	Atomic force microscopy

G. Purohit · D. S. Rawat (✉)
Department of Chemistry, University of Delhi, Delhi 110007, India
e-mail: dsrawat@chemistry.du.ac.in

S. Gulati (ed.), *Chitosan-Based Nanocomposite Materials*,
https://doi.org/10.1007/978-981-19-5338-5_3

CHI	Chitosan (CHI)
DLS	Dynamic light scattering
DMC/TPP	*N,N*-Dimethyl chitosan/tripolyphosphate
EDX	Energy-dispersive X-ray spectroscopy
ESCA	Electron spectroscopy for chemical analysis
ETAs	Electrothermal atomizers
FESEM	Field emitter scanning electron microscopy
FT-IR	Fourier-transform infrared spectroscopy
HCL	Hollow cathode lamp
ICDD	International Centre for Diffraction Data
ICP-MS	Inductively coupled plasma mass spectroscopy
JCPDS	Joint Committee on Powder Diffraction Standards
MW	Molecular weight
NMR	Nuclear magnetic resonance
NPs	Nanoparticles
PCS	Photon correlation spectroscopy
PLA/CS	Poly(lactic acid)/chitosan
QELS	Quasi-elastic light scattering
SEM	Scanning electron microscopy
TEM	Transmission electron microscopy
TMC/TPP	*N,N,N*-Trimethyl chitosan/tripolyphosphate
XPS	X-ray photoelectron spectroscopy
XRD	X-ray diffraction

1 Introduction

Chitosan (CHI), i.e., "cationic (1-4)-2-amino-2-deoxy-β-d-glucan" is a linear semicrystalline naturally occurring biopolymer/polysaccharide that is produced by deacetylation of homopolysaccharide "chitin" [1]. The primary source of chitosan is marine organisms, fungi-cell walls, and insects-exoskeletons which have major components containing glucosamine and N-acetyl glucosamine associated via β-(1-4) linkages. During the chitin-deacetylation process, a segment of the N-acetyl groups is lost in an alkaline medium, and this polysaccharide is named chitosan (CHI) possessing D-glucosamine-derived chitin units. The process of chitin-deacetylation can be performed either by using enzymatic hydrolysis (chitin deacetylase) or under alkaline conditions using a blend of anhydrous hydrazine-hydrazine sulfate or potassium/sodium hydroxide solutions. Only in an acidic medium, this CHI is soluble and positively charged. When the pH of CHI crosses its pKa value (≈6.5), the polymeric chitosan dissipates its positive charge and precipitates, making it a pH-responsive material [2]. The presence of abundant amino and highly reactive hydroxyl functionalization on the chitosan backbone enhances its chelating ability and polyelectrolytic nature. Such elusive properties of chitosan make it soluble only in a dilute acidic

solution and insoluble in water or any other organic solvents. Chitosan also exhibits antifungal, antimicrobial, analgesic, hemostatic, and mucoadhesive properties. The origin of the chitin source and deacetylation method alters the structural properties of chitosan, viz., molecular weight (MW), and the degree of deacetylation. The low toxicity, biocompatibility, and biodegradability of chitosan and its derived nanoparticles have attracted the attention of academicians/researchers due to its potential applicability in the renowned areas, viz., agriculture, engineering, biotechnology, pharmaceuticals, etc. Chitosan nanomaterials in comparison to bulk counterparts exhibit an array of applications due to their high surface-to-volume ratio, smaller size, cationic nature, etc. The processed metal encapsulated, or naked chitosan nanomaterials could be of various shapes and sizes such as nano vehicles, nanoparticles (NPs), nanofibers/meshes, 3D scaffolds, nanocapsules, etc. [3]. These altered chitosan-based nanoparticles (NPs) have been studied for disease control and growth-promoting agents in numerous plant species, thereby displaying superior biological activity compared to their bulk/micron-sized chitosan counterparts/substrates. The multi functionalities of chitosan biopolymers make them special as for other biopolymers such vast applicability has not yet been reported in the literature. There are several synthetic strategies are reported in the literature using which chitosan nanoparticles or nanocomposites can be achieved such as solvent casting, ionic gelation method (cross-linking reaction), electrospinning, layer-by-layer (LbL) depositions, freeze-drying, etc. Before making use of synthesized chitosan NPs for various applications it is required to characterize the material fully. The topological properties, surface/particle appearance, charges, particle size, elemental composition, interactions among each other, etc., can be determined by making use of physicochemical and morphological characterization techniques [1–3]. This chapter broadly and exclusively discusses a series of techniques, viz., transmission electron microscopy (TEM), scanning electron microscopy (SEM), energy-dispersive X-ray spectroscopy (EDX), dynamic light scattering (DLS), X-ray diffraction (XRD), X-ray photoelectron spectroscopy (XPS), atomic absorption spectroscopy (AAS), inductively coupled plasma mass spectroscopy (ICP), fourier-transform infrared spectroscopy (FTIR), atomic force microscopy (AFM), nuclear magnetic resonance (NMR), etc., used for precise characterization of chitosan-based nanomaterials/nanoparticles.

2 Nanomaterial Properties

2.1 Morphological and Topological Properties of Chitosan Nanomaterials

The morphological, internal arrangement/architecture, surface topography, degree of aggregation, chemical identification, and particle size of chitosan NPs can be evaluated by making use of transmission electron microscopy (TEM), or cryo-TEM or scanning electron microscopy (SEM).

2.1.1 Scanning Electron Microscopy (SEM)

Scanning electron microscopy (SEM) is a valuable tool that determines the surface visualizations, in-depth study of functionalized/agglomerated chitosan (CHI) nanoparticles (NPs), and estimates the sample composition via energy-dispersive X-ray spectroscopy EDX. SEM uses an energized electron beam (typically 1–30 eV) which scans the surface of the sample in a raster pattern wherein the secondary emitted electrons or backscattered electrons are detected, thereby achieving resolutions in the nanometre range.

Depending on the nature of the sample (chitosan nanomaterials), the electronic interaction with the sample varies, resulting in various types of emitted electrons at or on the sample surface. The detected electrons of different energies are processed and displayed as a pixel in the monitor, thereby visualizing 3D images or composition of nanomaterials (refer to Fig. 1). When these electrons are beamed under a high electric field, it is then popularly known as field emitter scanning electron microscopy (FE-SEM) [4–6]. Conventionally, to improve the electrical conductivity and contrast of nanomaterials, ultrathin coating with noble metals, viz, gold (Au), silver (Ag), and platinum (Pt) are used under high vacuum surroundings [7].

The application of SEM analysis for having a pictorial visualization is extensively used in literature for CHI-based nanomaterials/NPs [7]. In 2010, Dev et al. reported the synthesis of poly (lactic acid)/chitosan "PLA/CS" NPs using emulsion and solvent evaporation techniques [8]. Figure 2a shows the SEM images of PLA/CS NPs at different magnifications, wherein these particles' surface morphology is spherical [8]. Hosseini et. al 2013 prepared the essential oil encapsulated chitosan NPs using a two-step process of oil-in-water emulsion preceded by ionic gelation [9]. The morphology of prepared chitosan NPs found to be spherical in nature which is nicely intact and had a clear distribution among themselves as evident from Fig. 2b [9].

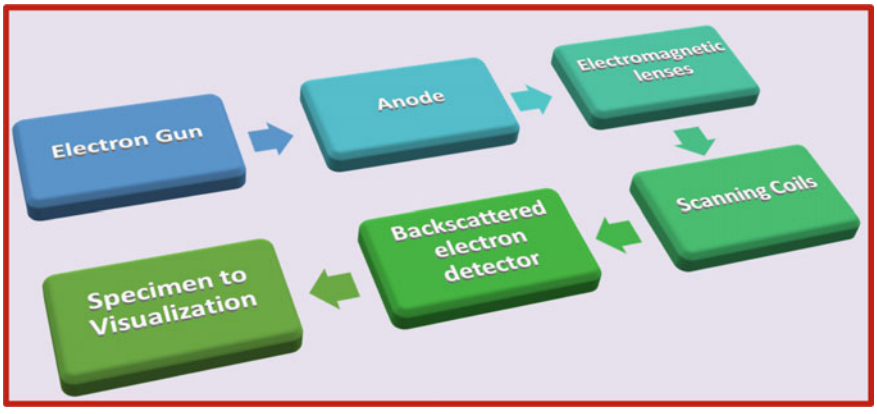

Fig. 1 Flowchart representing an overview of the SEM analysis process [4–6]

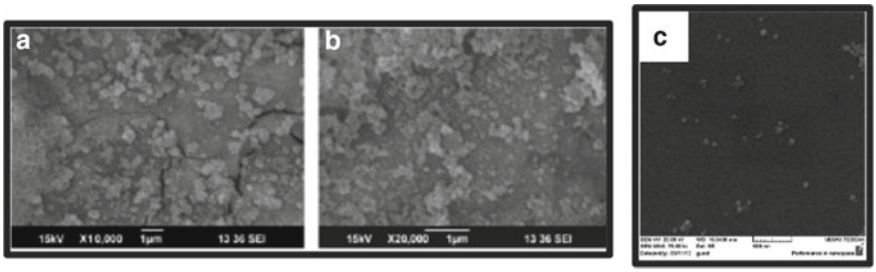

Fig. 2 SEM images of **a** poly-lactic acid/chitosan "PLA/CS NPs" [8] Reproduced from Dev et al. with permission from Elsevier **b** chitosan NPs [9] Reproduced from Hosseini et al. with permission from Elsevier

2.1.2 Transmission Electron Microscopy (TEM)

The higher spatial resolution, i.e., equivalence with the atomic dimensions makes transmission electron microscopy "TEM" quite a popular technique to characterize chitosan-based nanomaterials, which provides chemical information and internal structural arrangements in an image form. In TEM, a highly energized beam of electrons passes via a thin foil wherein the electrons are transformed into elastic/inelastic electrons which then interact with the specimen containing a sample of chitosan nanomaterial. The interactions of those inelastic/elastic electrons with the specimen gave rise to the emission of reflected/transmitted particles. The difference in energies is then detected and used to generate the higher resolution magnified images captured by the camera followed by visualization in a monitor. It is noteworthy to mention that ratio between the specimen, image plane, and the objective lens is taken into account which has to be magnified by the lens (Fig. 3a) [10, 11].

Although both SEM and TEM depicts the visualization of nanomaterial, i.e., how it looks, how the atoms are arranged, the extent of aggregation, and information on particle size/dimension but when compared to each other TEM is advantageous in proving higher resolution (as low as 0.2 nm) with good quality analytical measurements. TEM provides detailed information as it utilizes the energetic electrons which can be used to infer the composition, morphological, imaging, and crystallographic analysis. Therefore, TEM used three main techniques, i.e., electron microscopy, imaging, and diffraction pattern (Fig. 3b). Sample preparation in the case of TEM aialysis is quite simple, wherein before analysis a drop or two of suspension of chitosan-based nanomaterials (after sonication) is placed into a carbon-coated copper grid followed by drying or sometimes IR irradiation. TEM also distinguishes between the monocrystalline, polycrystalline, and amorphous chitosan-based nanomaterials/NPs [10]. It is noteworthy to mention that the size distribution or size estimation using TEM of nanomaterials is precise, not accurate as the chances of aggregation can occur during the evaporation of the sample preparation process. Cryo-TEM is superior to usual TEM analysis as in the former case, by using cryogenic temperature

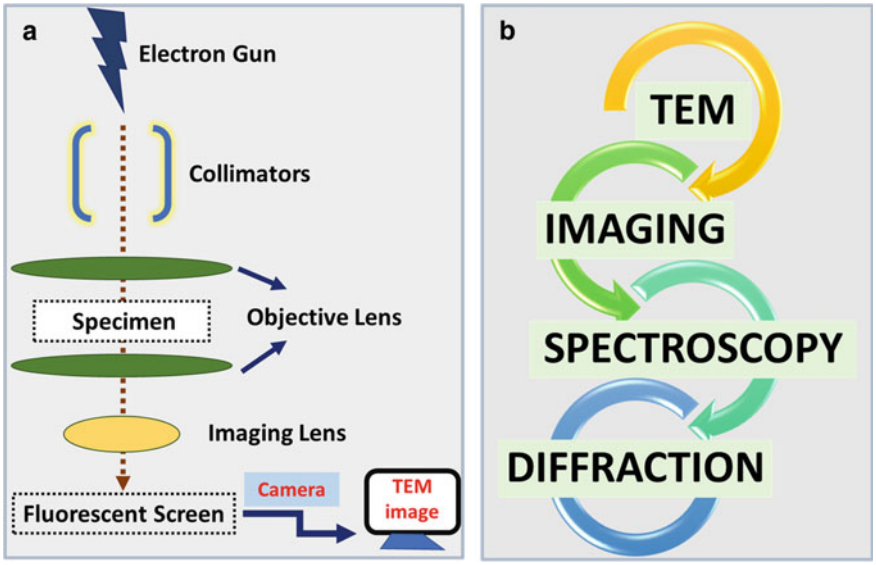

Fig. 3 **a** Flow chart representing steps involved in working principle of TEM analysis [10, 11]; **b** Three main techniques of TEM [11]

(−100 to −175 °C) a suspension of nanomaterial is solidified, and the visualization is done when the specimen is in the frozen state. The aforementioned method bypassed the problem of nanoparticle aggregation, usage of heavy-metal contrasting agents, and solvation thus giving not only precise but also predicting an accurate size estimation [11]. Cryo-TEM is particularly useful when one must distinguish whether the chitosan-based nanomaterials have the natural tendency of self-assembly or if it only occurs during sample preparation wherein solvation/evaporation procedures came into the picture [11–13]. In the literature, numerous reports have mentioned the use of TEM analysis for chitosan-based nanomaterials/NPs. Facchi et al., (2016) successfully reported the synthesis of *N*-modified chitosan NPs for curcumin delivery using a benzyl alcohol/water emulsion system (Fig. 4) [14]. Figure 4a–d shows the TEM analysis of *N,N,N*-Trimethyl chitosan/tripolyphosphate (TMC/TPP) and *N,N*-dimethyl chitosan/tripolyphosphate (DMC/TPP) NPs which have irregular spherical geometries attributed to vigorous stirring while using the benzyl alcohol/water emulsion system [14]. TEM analysis also tells that the average particle size for DMC/TPP NPs is up to 317 nm, while for TMC/TPP NPs it is ~99 nm [14].

In the year 2002, Banerjee et al. reported the synthesis of ultrafine chitosan nanoparticles wherein, the amine groups are cross-linked (10% or 100%) using a reverse micellar system containing surfactant, i.e., sodium bis(ethylhexyl) sulfosuccinate (AOT) and *n*-hexane [15]. The TEM analysis depicts the particles are shaped spherically and are aggregated with the dimensions of 30 nm when 10% amine functionalization (for chitosan NPs) is cross-linked whereas with 100% cross-linking the particle size shoots up to 110 nm (Fig. 4e, f [15]. Numerous other reports too

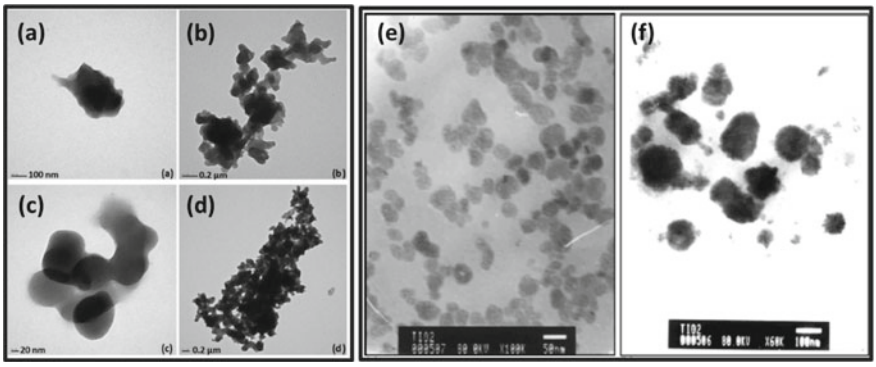

Fig. 4 TEM images of **a**, **b** DMC/TPP [14] Reproduced from Facchi et al. with permission from Elsevier; **c**, **d** TMC/TPP chitosan nanoparticles [14] Reproduced from Facchi et al. with permission from Elsevier; **e** 10% [15] and **f** 100% cross-linked chitosan nanoparticles [15] Reproduced from Banerjee et al. with permission from Elsevier

showed spherical kind morphologies of chitosan-based NPs [16–18] and also with metal encapsulation such as Cu with chitosan [19, 20].

2.2 Solid-State Properties of Chitosan-Based Nanomaterials/NPs

Like every other nanoparticle system, chitosan-based nanomaterials/NPs are not elementary molecules rather they are configured as three main layers. The first and foremost is the surface layer wherein a suitable functionalization can be done, encapsulating metal ions within, coating with surfactants, etc. The second layer, i.e., the middle layer/shell layer is chemically distinct followed by the third layer which is essentially the core and is the central/innermost segment of chitosan-based NPs. To identify the crystallinity, composition, defect structure, grain size, etc., all are solid-state properties that can be effectively useful to elucidate the molecular dynamics of chitosan-based nanomaterials/NPs. X-ray diffraction (XRD) is a powerful tool that can be used to study the solid-state properties of chitosan-based nanomaterials/NPs [1, 21, 22].

2.2.1 X-ray Diffraction (XRD)

In material science, it is an extremely important aspect to determine the crystallographic structure of nanomaterials. In the year of 1912, Max Von Laue made an important discovery that the two-dimensional diffraction gratings of a substance (nanomaterial/NPs) in presence of X-ray wavelength act in a similar fashion to that

of plane spacing in a crystal lattice. XRD is a non-destructive analytical technique that solves the purpose of surface/phase identification of chitosan-based nanomaterials, thereby giving information on cell dimensions and atomic spacings as well. In XRD (Please refer to Fig. 5), the incident X-rays (generated by cathode ray "Cu X-ray tube" with 1.5418 Å) are filtered to produce monochromatic radiation which was then collimated to concentrate and are used to irradiate the sample (chitosan-based nanomaterial) [23–25].

Upon satisfying Bragg's law ($n\lambda = 2d \sin\theta$), the interaction between the incident rays and chitosan-based nanomaterial produces a constructive interference followed by a diffracted ray. Bragg's law correlates the wavelength of an incident ray "λ" proportional to that of diffraction angle "θ" and lattice spacing "d", thereby measuring the respective intensities and scattering angle that is diffracted from the sample [23, 24]. The sample material which is chitosan-based nanomaterial must be homogenized be it in a film form or finely grounded powdered form. By changing the 2θ (2 theta) angles to all plausible ranges, a finite diffraction direction of the lattice can be attained. Each material has a specific unique set of d-spacings whose corresponding positions/intensities are available from International Centre for Diffraction Data (ICDD) or in earlier times known as Joint Committee on Powder Diffraction Standards JCPDS data as a reference pattern/database [23]. Thus, by converting diffraction peaks to d-spacings one can easily identify the grain size, composition, shape of a unit cell, crystalline nature, etc., of chitosan-based nanomaterials/NPs [24–27]. It is noteworthy to mention that the diffraction angle direction depends on the nature, shape, and size of a unit cell of chitosan-based nanomaterials/NPs, whereas the intensities of diffraction patterns depend on the structural internal arrangements of the atoms.

Rhim et al. (2006) successfully reported the XRD spectra of chitosan powder wherein, a characteristics peaks corresponding to 2θ values of 10.9° and 19.8° which corresponds to the amorphous structure of chitosan (Fig. 6d, black graph) [28].

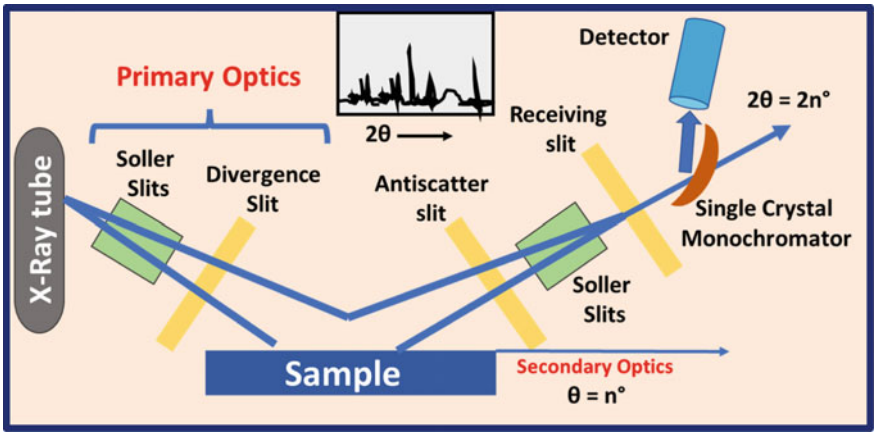

Fig. 5 Working principle of X-ray spectroscopy [23–25]

Whereas, after chemical processes, the as-synthesized chitosan nanofilm showed a characteristic peak of 2θ values of 8°, 11° corresponds to the hydrated crystalline structure of chitosan nanofilm and 18° to amorphous characteristics (Fig. 6d, blue graph) [28] It is well known in the literature that the structural modifications of chitosan alter its internal lattice structure arrangements. Factors such as the dissolution process, drying, precipitation, processing chemical treatment, molecular weight, degree of deacetylation, etc., cause the changes in chitosan structural arrangements [28]. Furthermore, Hosseini in 2013, recorded the XRD patterns of OEO-loaded chitosan nanoparticles over a 2θ range of 5–50°, and it showed the characteristic peak corresponding to 2θ of 25° indicating a high degree of crystallinity (Fig. 6a–c) [29]. As shown in Fig. 6a–c, the broad peak in the XRD spectrum indicated the cross-linking reactions between chitosan and TPP. This proves that the chitosan NPs are having a densely packed network structure corresponding to the interpenetrating polymeric chain of chitosan with TPP counterparts [29]. XRD diffractograms of chitosan-based nanomaterials are reported in literature many times [30–33] For example, metal encapsulated on chitosan, i.e., Cu-chitosan NPs shows a characteristic 2θ range between 19.5 and 21.0 which corresponds to the crystalline nature of Cu-chitosan NPs system [34].

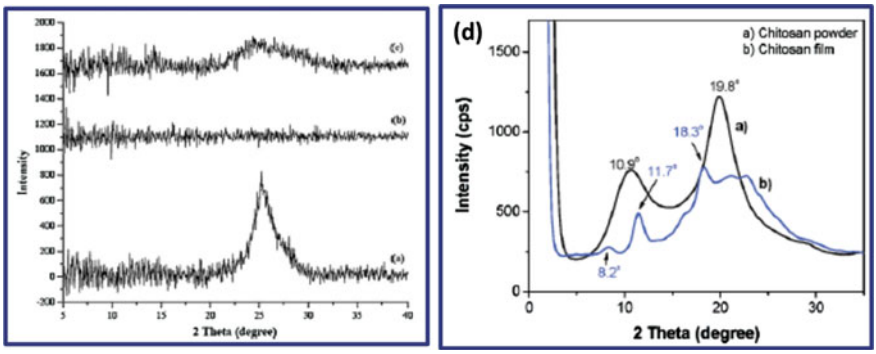

Fig. 6 XRD spectra of **a** chitosan powder [29] Reproduced from Hosseini et al. with permission from Elsevier **b** chitosan nanoparticles [29] Reproduced from Hosseini et al. with permission from Elsevier **c** OEO-loaded chitosan NPs [29] Reproduced from Hosseini et al. with permission from Elsevier **d** comparison between chitosan powder (black graph) and chitosan film (blue graph) [28] Reproduced from Rhim et al. with permission from Elsevier

2.3 *Elemental Analysis/Properties of Chitosan-Based Nanomaterials/NPs*

2.3.1 X-ray Photoelectron Spectroscopy (XPS)

X-ray photoelectron spectroscopy "XPS" is one of the prominent surface science techniques with which one can infer/analyze the chemical state, electronic states, and elemental composition/empirical formula of nanomaterials. In the year 1887 Hz, discovered the photoelectric effect which is the basis of the XPS working principle. Later in the 1960s, Siegbahn and his research group at Uppsala University, Sweden extended this work to surface analysis and coined the term XPS or ESCA (electron spectroscopy for chemical analysis) for which Siegbahn won a noble prize in physics in 1981 [35, 39, 43].

As shown in Fig. 7a, XPS, a qualitative analysis involves the bombardment of the sample with single energy or monochromatic or monoenergetic X-ray photons (Mg Kα 1253.6 eV or Al Kα 1486.6 eV, line width $\approx$0.7–0.85 eV), followed by computing the kinetic energy of emitted electrons from the topmost layer of the sample (1–10 nm) [35]. The electrons which are emitted from outermost/surface atoms have characteristic peaks in the XPS spectrum, thereby enabling one to identify and quantify the surface elements present (except hydrogen and helium). The chemical states of elements present within can be identified and quantified simply by measuring/investigating the minute variations occurring in binding energies of emitted photoelectrons, auger electrons, multiple splitting, satellite peaks, etc. (Please refer to Fig. 7b). It is important to mention that an XPS spectrum is plotted as the relative number of electrons against their respective binding energies (eV). XPS is an ultra-high vacuum and sensitive technique that changes in the electronic configuration of the atoms or chemical bonds can be easily detected thereby the existence of certain elements or species can be identified. In the case of chitosan-based nanomaterials, the determination of elements such as C, N, O and P can be easily identified as these elements constitute the majority and have characteristic peaks corresponding to their respective binding energies [36]. Boufi et al. in 2013 reported the XPS for the mild-wet synthesized gold/silver NPs in an aqueous chitosan solution [35]. Figure 8a–b shows the survey XPS spectra and N 1a XPS region of chitosan nanoparticles (blue spectrum) which clearly indicates the presence of N 1s whose peak corresponds to the binding energy of 399.4 ± 0.2 eV. The binding energy value of 399.4 is characteristic of nitrogen in NH_2 groups or NH-CO groups indicating a mixed chitosan-chitin structure [35].

Trapani et al. (2011) demonstrated the XPS spectra of chitosan nanoparticles [36]. Figure 9a–b shows the high-resolution C1s XPS spectra wherein the typically observed ratio of 3.8 of binding energies values of 286.5 and 288.0 eV corresponds to CS (chitosan bulk, Fig. 9a) and CSNPs (chitosan nanoparticles, Fig. 9b) [36]. Moreover, Fig. 9f–g shows the curve fitted N 1s high-resolution regions of XPS spectra for chitosan and chitosan NPs wherein the lower binding energy value of 399.6 eV, 401.1 and 402.0 eV corresponds to the aminic group, amide group, and

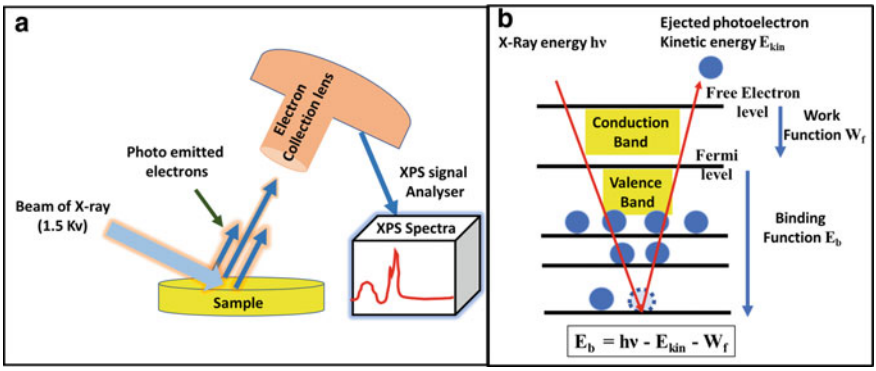

Fig. 7 Schematic representation of **a** XPS process and **b** basic working principle of XPS involving auger process and photoemission [35, 36]

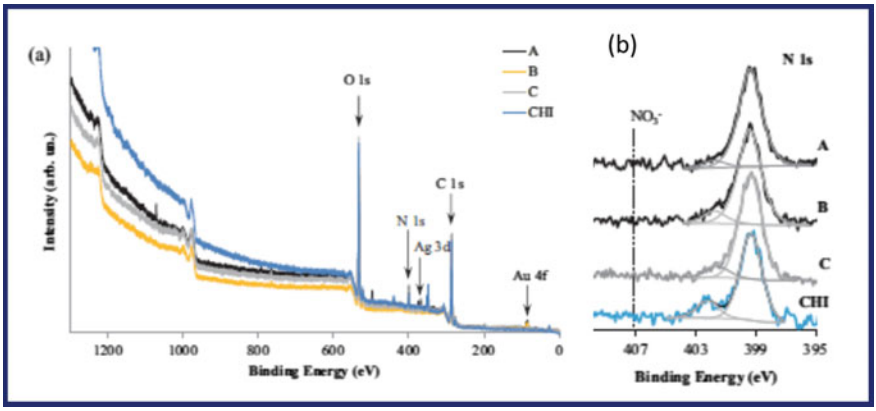

Fig. 8 **a** XPS survey spectra of chitosan NPs (blue graph, –CHI); **b** XPS N1s regions of CHI NPs (blue graph) [35] Reproduced from Boufi et al. with permission from Elsevier

protonated quaternary nitrogen, respectively [36]. Many other prominent research groups reported the XPS data for chitosan and chitosan-based nanoparticles which are modified by encapsulating such as copper or chitosan aerogels [37–43].

2.3.2 Atomic Absorption Spectroscopy (AAS)

To determine the metal concentration at the pictogram level in a variety of samples, atomic absorption spectroscopy "AAS" is used which is an extremely sensitive technique for elemental analysis [44]. In AAS, the reduction in the intensity of optical radiation of cell containing gaseous atoms of samples are measured. Typically, in AAS, an analyte absorbs specific wavelengths emitted by a hollow cathode lamp

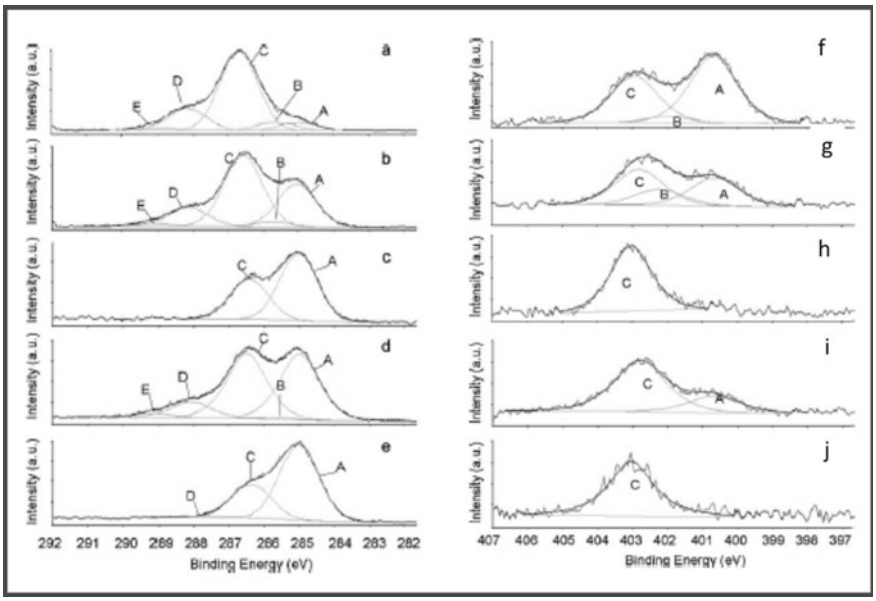

Fig. 9 XPS of **a** C1s regions of pure CS; **b** C1s regions of CSNPs; **f** N1s regions of pure CS; **g** N1s regions of CSNPs [36] Reproduced from Trapani et al. with permission from Elsevier

"HCL" which is used as a light source as shown in Fig. 10 [45, 46]. In AAS, either the flames or graphitic-furnaces/electrothermal atomizers "ETAs" are commonly used atom-cells. The sensitivity of flames is relatively less than that of ETAs as in the case of ETAs the temperature can be supervised by a power supply, whereas flames consist of a meticulously controlled combustion environment. To prevent the process of combustion at elevated temperatures the use of inert gas such as argon is employed. On absorbing the particle wavelength, the sample/analyte in an "atom-cell" turns into a gaseous state which then travels to a detector whose job is to quantify and isolate the wavelengths of interest followed by processing the data in a computer/control instrumentation operation. To provide optimal accuracy, precision, and minimal interferences, the analyte or samples are made by digestion procedures and are usually of specific concentration in an aqueous phase [46].

It is important to mention that every single element absorbs wavelengths of electromagnetic radiation for HCL source differently. In other words, the absorbance of elements is extremely specific and particular for the absorbing wavelength of interest and is measured against the standards. When the standards are measured, it implies that the instrument is calibrated for particular elements of interest, and hence the unknown sample can be processed, and the concentration can be obtained from the digital output display unit. The basic phenomenon involved in AAS is the concept of ionization energy which is basically the energy required to excite an electron and is particular for each element. In the case of chitosan-based nanomaterials/NPs,

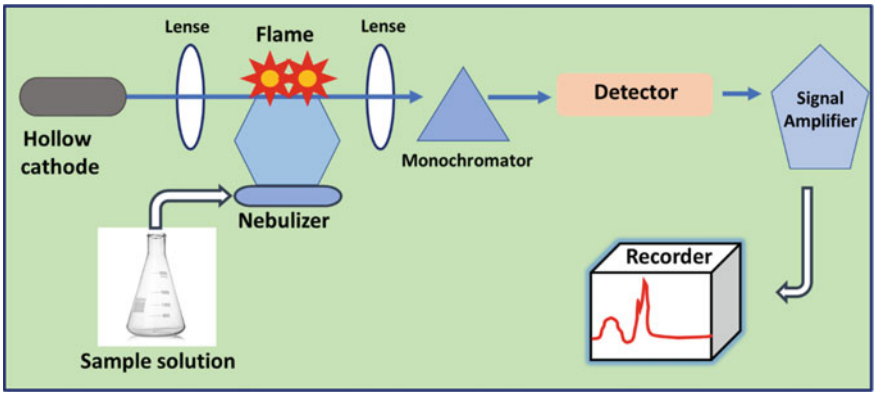

Fig. 10 Schematic representation of atomic absorption spectroscopy (AAS) [45, 46]

every atom has its own distinctive fingerprint regions, enabling the qualitative AAS analysis of the material [47–49].

Chitosan-based nanomaterials have been widely used to encapsulate the metal ions and hence the AAS analysis can be done against different reaction parameters too such as agitation time, rate of reaction, pH, etc. [19, 50, 51]. In general, the Concentration of encapsulated metals (%) can be calculated by taking the ratio of the amount of released metal ions to the total amount of metals present in a nanomaterial followed by multiplying it by 100. Liu et al. in 2002, demonstrated the use of chitosan-based nanomaterials for the metal encapsulation, and the amount of metal ions was then evaluated by making use of AAS technique [52]. Figure 11 shows the relative percentage of absorbance of metal ions such as Ca^{2+}, Zn^{2+}, Ag^{+}, Cr^{3+}, and Mg^{2+}, on the chitosan-modified glass beads using the AAS spectroscopy [54].

2.3.3 Inductively Coupled Plasma Mass Spectroscopy (ICP)

In inductively coupled plasma mass spectroscopy "ICP-MS" an inductively coupled plasma is used to atomize the sample. Upon atomization, it creates atomic and small-polyatomic ions which were then detected. Figure 12 shows a schematic representation of a single quadrupole of IC-MS which has six major slots/compartments [53]. It starts with a sample solution in an introduction system which is then processed into a nebulizer followed by an inductively coupled plasma in the presence of inert gas for say Argon. The highly ionizable plasma then atomizes the sample thereby generating the polyatomic ions (fine aerosol form) which then using ion optics were extracted to an interface region. The electrostatic lens of ion optic focuses the polyatomic ions into a quadrupole mass analyzer.

In accordance with the mass by charge ratio "m/z ratio" the detection and separation of ions take place. For instance in ICP-MS, the samples which are to be analyzed are digested in a similar fashion in an aqueous phase as it is done in the case of AAS

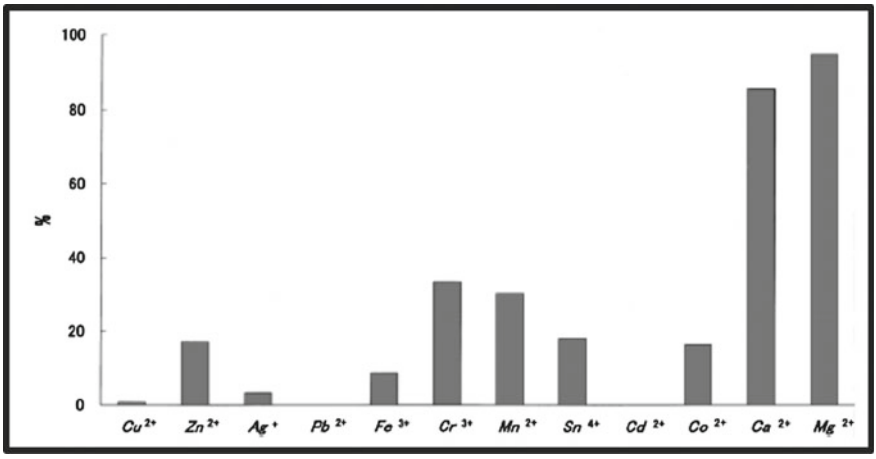

Fig. 11 The metal ion adsorption rate of the chitosan-modified glass beads using AAS [54] Reproduced from Liu et al. with permission from Elsevier

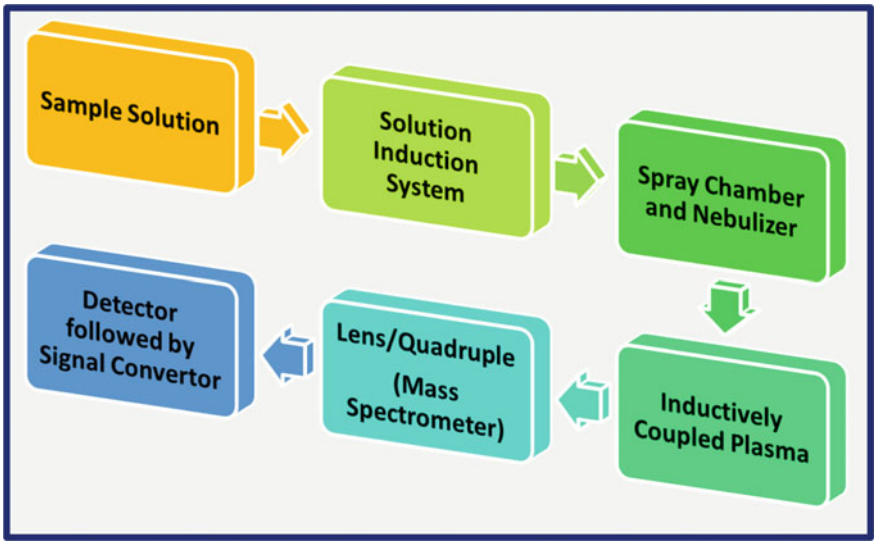

Fig. 12 Schematic representation demonstrating steps involved in ICP analysis [53]

sample preparation case too. The sample preparation includes the use of hydrochloric or nitric acid or in some cases alkaline solutions too and diluent is deionized water [53]

There are not many reports in the literature that explain the use of ICP-MS on chitosan-based nanoparticles. Although, ICP-MS proves to be an effective and supportive technique for the estimation of metal ions bound or formed using

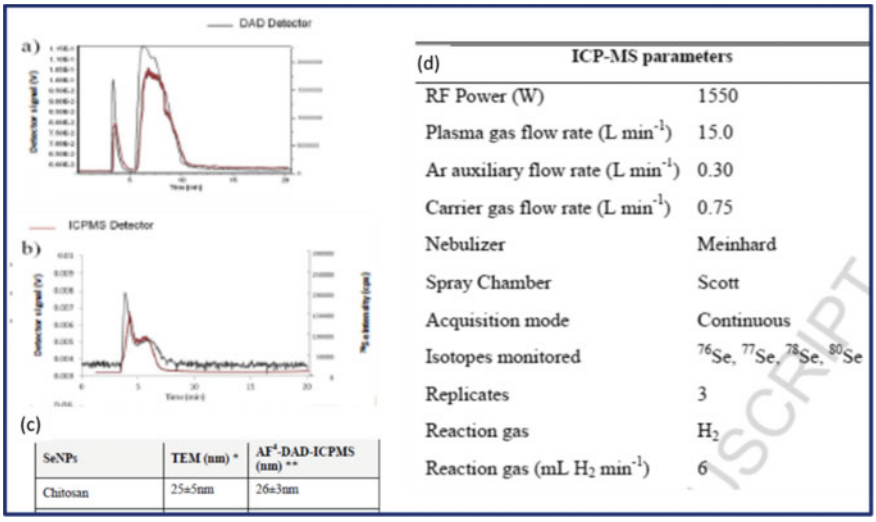

Fig. 13 **a**, **b** The fractograms showing the fractionation of Se NPs prepared in chitosan and Triton X-100 **c** TEM size estimation of SE NPs and AF^4-DAD-ICP-MS **d** Operating conditions for AF^4-DAD-ICP-MS [58] Reproduced from Palomo-Siguero et al. with permission from Elsevier

chitosan-based nanomaterials [54–57]. Palomo-Siguero et al. in 2017 synthesized the Selenium NPs using a solution-phase strategy in presence of stabilizers such as chitosan(polysaccharides) or non-ionic surfactant (Triton X-100) [58]. Figure 13a–d shows the ICP-MS fractograms of fractionization of Se NPs synthesized by using chitosan and Triton X-100 stabilizers [58]. The selenium peaks were identified by using ICP-MS whose operating conditions for running ICP-MS are shown in Fig. 13d [58].

2.4 Interaction Analysis/Properties of Chitosan-Based Nanomaterials/NPs

The type of bonds present within the chitosan-based nanoparticles and their interaction/functional group analysis is an important aspect that tells the kinds of specific bonds present within the system. To measure such properties that include the guided alterations and modifications, fourier-transform infrared spectroscopy is an indispensable tool to study the same.

2.4.1 Fourier-Transform Infrared Spectroscopy (FT-IR)

Fourier-transform infrared spectroscopy "FTIR" is a chemical identification technique that gives insightful information on the interaction of bonds with their corresponding functionalities.

The underlying principle of the FTIR technique is based on the absorption of electromagnetic radiation of the infrared region (4000–400 cm^{-1}) by a molecule (inorganic/organic). For a molecule to be IR active, the dipole moment should change on absorbing IR radiation, and it becomes IR active. Figure 14 shows the schematic representation demonstrating steps involved in FT-IR analysis wherein the frequency is measured in terms of wavenumbers, and the data is recorded in the form of an interference pattern which is then converted into a spectrum (transmittance/absorbance form) [59]. The spectrum is usually in the form of distinct lines that could be narrow or broad and corresponds to a specific frequency thereby helping in identifying the nature of bonds, functionalities pertaining to molecular structures, and interactions [59]. The samples could be of any type (liquid, solid, or gaseous), but in general solid or liquid samples are prepared using KBr (100: 1), and the pellet is made by using a hydraulic press machine. Initially, at room temperature, the instrument is calibrated by recording a blank KBr background followed by a KBr pellet containing the samples of our interest let's say chitosan nanomaterial/NPs in an absorbance/transmittance mode. It is worth mentioning that the FTIR technique is quite an impressive analytical tool that helped in understanding the functionalities of chitosan-based nanomaterials/NPs [8, 60–65].

Banerjee et al. in 2002 characterized the chitosan NPs using FTIR analysis. The chitosan NPs were synthesized by cross-linking reaction between the chitosan polymer and glutaraldehyde using the reverse micellar technique [66]. Figure 15a–b shows the FTIR spectra for chitosan and chitosan NPs. It may be noted that in Fig. 5b,

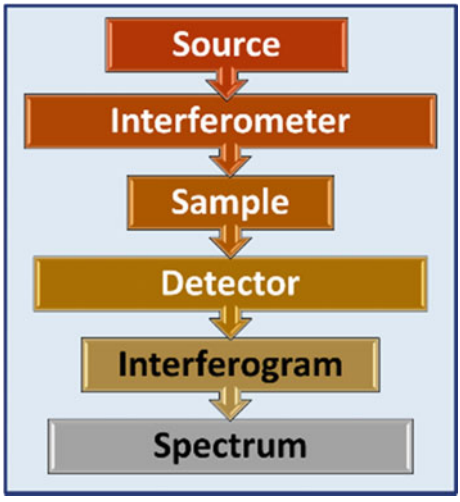

Fig. 14 Schematic representation demonstrating steps involved in FT-IR analysis [59]

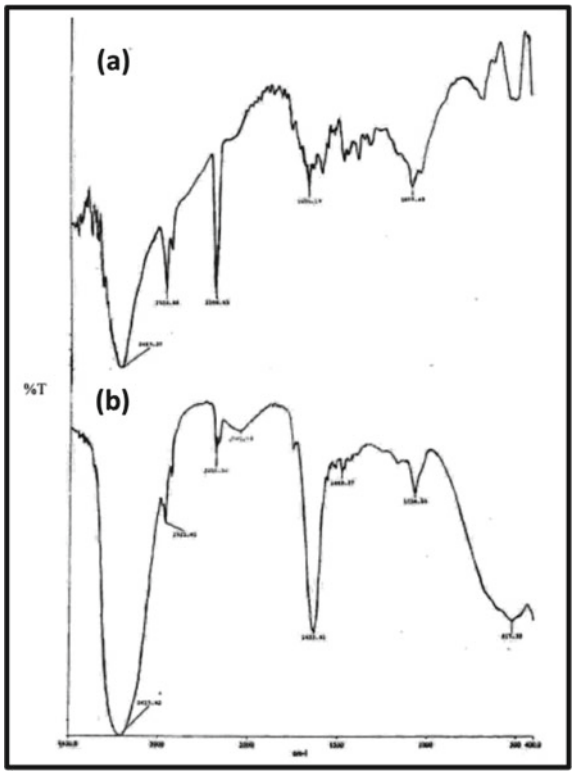

Fig. 15 FTIR spectra of **a** chitosan polymer and **b** cross-linked chitosan nanoparticles [66] Reproduced from Banerjee et al. with permission from Elsevier

an additional peak at 1634 cm^{-1} is in agreement with the stretching vibrations of C = N, elucidating cross-linked chitosan NPs [66]. Moreover, a peak at 1650 cm^{-1} corresponds to the scissoring vibrations of NH_2 of primary amines in chitosan chains. The peaks around 1020–1075 cm^{-1} imply the symmetric stretch of C–O–C bonds and 2926 cm^{-1} manifested the string polymeric backbone C–H vibrations [66].

2.5 Determination of Chitosan-Based Nanomaterials/NPs

For chitosan nanoparticles determining topological properties such as surface charge, particle size distribution, as well as particle size, can be evaluated by the dynamic light scattering "DLS" technique.

2.5.1 Dynamic Light Scattering (DLS)

Dynamic light scattering (DLS) or photon correlation spectroscopy (PCS) or quasi-elastic light scattering (QELS) is a versatile and powerful tool to examine the

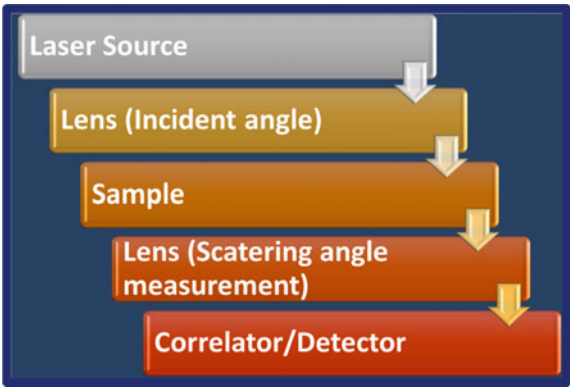

Fig. 16 Schematic representation of dynamic light scattering [67]

diffusion behavior of molecules in the solution phase. The hydrodynamic radii or diffusion coefficient is calculated in the DLS or PCS technique, which defers the size distribution, particle size, surface charge, and shapes of particles (nanoparticles/macromolecules) [67]. Typically, in DLS, the sample to be analyzed has to be in a solution phase, and hence the size is estimated by studying the Brownian motion of suspended particles having different scattered angles 'θ' (Refer Fig. 16) [67]. The random motion of suspended particles/molecules is because of the continuous bombardment by the solvent molecules around them. Using the DLS technique, one can measure the particles in the submicron region and of the dimension of <1 nm. In DLS, the size of the NPs was calculated using Stoke-Einstein equation. The size of chitosan NPs/nanomaterials which is hydrodynamic radii "d_h" can be determined from the diffusion of particles "D", i.e., $d_h = kT/3\pi\eta D$ wherein k is Boltzmann constant, η is the viscosity of the medium, and T is the absolute temperature [67].

Much scientific work is already reported in the literature where the DLS technique proves to be an important aspect to determine the size distribution as well as surface charge properties [14, 68, 69]. To get reliable data, it is important to combine the more sophisticated techniques such as microscopy with the DLS technique. For fully dispersed chitosan nanoparticles/nanomaterials reliable as well as reproducible data can be obtained wherein the concept of aggregation can be eliminated. Banerjee et al. in 2002 reported the DLS data of chitosan nanoparticles as shown in Fig. 17a [66]. Since the underlying principle of the DLS technique is based on the Brownian motion of particles and chitosan is polymeric in nature hence the actual size is always lesser than the observed average particle size. Li et al. in 2008 estimated the average particle size distribution of ferrite-coated chitosan NPs using the DLS technique wherein the size varies from 10 to 100 nm as shown in Fig. 17b [70].

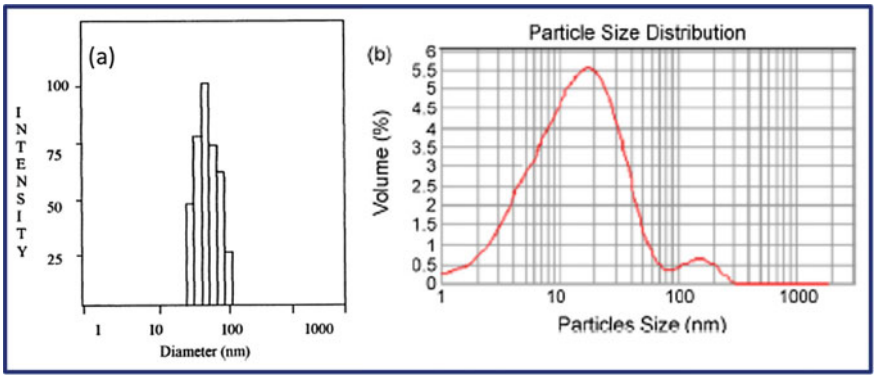

Fig. 17 **a** Size distribution of chitosan nanoparticles by QELS [66] Reproduced from Banerjee et al. with permission from Elsevier **b** Particle size distribution of the Fe_3O_4–chitosan nanoparticles [70] Reproduced from Li et al. with permission from Elsevier

3 Conclusion

Chitosan-based nanomaterials/NPs have gained attention in recent times and have shown exponential growth specifically in the area of medical sciences and agriculture. Characterizing the chitosan-based nanomaterials/NPs provides reliability, accuracy, and consistent results especially to understand the nanomaterials and their sustainability. The important characterizing tools such as SEM, TEM, Cryo-TEM, XRD, XPS, AAS, ICP, FTIR, and DLS help in understanding the chemical and physical properties of chitosan-based nanomaterials/NPs. Therefore, representing the role of each technique in a conclusive manner will help the scientific community to understand the properties of chitosan-based nanomaterials/NPs. In this way, it will be beneficial for researchers, academicians as well as students to select and understand the most suitable technique of their choice to assess their uses in a precise manner.

References

1. Mourdikoudis S, Pallares RM, Thanh NTK (2018) Characterization techniques for nanoparticles: comparison and complementarity upon studying nanoparticle properties. Nanoscale 10:12871
2. Qu B, Luo Y (2021) A review on the preparation and characterization of chitosan-clay nanocomposite films and coatings for food packaging applications. Carbohydr Polym Technol Appl 2:10010
3. Choudhary RC, Kumari S, Kumaraswamy RV, Pal A, Raliya R, Biswas P, Saharan V (2019) Characterization methods for chitosan-based nanomaterials. In: Prasad R (eds) Plant nanobionics. Nanotechnology in the life sciences. Springer, Cham. https://doi.org/10.1007/978-3-030-12496-0_5
4. McMullan D (1995) Scanning electron microscopy 1928–1965, Scanning 17, pp175–185. https://doi.org/10.1002/sca.4950170309

5. Ponomarev A, Yudovich M, Nikitin V, Nikitin D, Barchenko V, Sobol' V (2000) Some features of analysis of solutions of fullerenes C60 and C70 by their absorption spectra. Optics Spectrosc 88:195–196
6. Saharan V, Pal A (2016) Chitosan based nanomaterials in plant growth and protection. Plant Sci. https://doi.org/10.1007/978-81-322-3601-6_3
7. Choudhary RC, Kumaraswamy RV, Kumari S, Sharma SS, Pal A, Raliya R, Biswas P, Saharan V (2017a) Synthesis, characterization, and application of chitosan nanomaterials loaded with zinc and copper for plant growth and protection. In: Prasad et al (eds) Nanotechnology. Springer Nature Singapore Pte Ltd, Singapore
8. Dev A, Binulal NS, Anitha A, Nair SV, Furuike T, Tamura H, Jayakumar R (2010) Preparation of poly(lactic acid)/chitosan nanoparticles for anti-HIV drug delivery applications. Carbohydr Polym 80:833–838
9. Hosseinia SF, Zandib M, Rezaeia M, Farahmandghavi F (2013) Two-step method for encapsulation of oregano essential oil in chitosan nanoparticles: preparation, characterization and in vitro release study. Carbohydr Polym 95:50–56
10. Mourdikoudis RM, Pallares NTK, Thanh (2018) Characterization techniques for nanoparticles: comparison and complementarity upon studying nanoparticle properties. Nanoscale 10:12871–12934
11. Parupudi A, Mulagapati SHR, Subramony JA (2022) Chapter 1—Nanoparticle technologies: recent state of the art and emerging opportunities. In: Kesharwani P, Singh KK (eds) Nanoparticle therapeutics. Academic Press, pp 3–46. ISBN 9780128207574. https://doi.org/10.1016/B978-0-12-820757-4.00009-0
12. Kumar PS, Pavithra KG, Naushad M (2019) Chapter 4—Characterization techniques for nanomaterials. In: Thomas S, Sakho EHM, Kalarikkal N, Oluwafemi SO, Wu J (eds) Nanomaterials for solar cell applications. Elsevier, pp 97–124. ISBN 9780128133378. https://doi.org/10.1016/B978-0-12-813337-8.00004-7
13. Pennycook SJ (2005) Transmission electron microscopy. In: Bassani F, Liedl GL, Wyder P (eds) Encyclopedia of condensed matter physics. Elsevier, pp 240–247. ISBN 9780123694010. https://doi.org/10.1016/B0-12-369401-9/00582-9
14. Facchi SP, Scariot DB, Bueno PVA, Souza PR, Figueiredo LC, Follmann HDM, Nunes CS, Monteiro JP, Bonafé EG, Nakamura CV, Muniz EC, Martins AF (2016) Preparation and cytotoxicity of N-modified chitosan nanoparticles applied in curcumin delivery. Int J Biol Macromol 87:237–245
15. Banerjee T, Mitra S, Singh AK, Sharma RK, Maitra A (2002) Preparation, characterization and biodistribution of ultrafine chitosan nanoparticles. Int J Pharm 243:93–105
16. Liu H, Gao C (2009) Preparation and properties of ionically cross-linked chitosan nanoparticles. Polym Adv Technol 20:613–619
17. Saharan V, Mehrotra A, Khatik R, Rawal P, Sharma SS, Pal A (2013) Synthesis of chitosan-based nanoparticles and their in vitro evaluation against phytopathogenic fungi. Int J Biol Macromol 62:677–683
18. Yuwei C, Jianlong W (2011) Preparation and characterization of magnetic chitosan nanoparticles and its application for Cu(II) removal. Chem Eng Sci 168:286–292
19. Choudhary RC, Kumaraswamy RV, Kumari S, Sharma SS, Pal A, Raliya R, Biswas P, Saharan V (2017b) Cu-chitosan nanoparticle boost defense responses and plant growth in maize (Zeamays L.). Sci Report 7:9754
20. Brunel F, Gueddari NEE, Moerschbacher BM (2013) Complexation of copper (II) with chitosan nanogels: toward control of microbial growth. Carbohydr Polym 92:1348–1356
21. Khan I, Saeed K, Khan I (2019) Nanoparticles: properties, applications and toxicities. Arab J Chem 12:908–931
22. Boateng E, Chen A (2020) Recent advances in nanomaterial-based solid-state hydrogen storage. Mater Today Adv 6:100022
23. Wong-Ng W, McMurdie HF, Hubbard CR, Mighell AD (2001) JCPDS-ICDD research associateship (cooperative program with NBS/NIST). J Res Natl Inst Stand Technol 106:1013–1028

24. Gonon M (2021) Case studies in the X-ray diffraction of ceramics. In: Pomeroy M (ed) Encyclopedia of materials: technical ceramics and glasses. Elsevier, pp 560–577
25. Vishwakarma V, Uthaman S (2020) 9-Environmental impact of sustainable green concrete, In: Liew MS, Nguyen-Tri P, Nguyen TA, Kakooei S (eds) Micro and nano technologies, smart nanoconcretes and cement-based materials. Elsevier, pp 241–255
26. Sima F, Ristoscu C, Duta L, Gallet O, Anselme K, Mihailescu IN (2016) 3-Laser thin films deposition and characterization for biomedical applications. In: Vilar R (ed) Laser surface modification of biomaterials. Woodhead Publishing, pp 77–125
27. Bunaciu AA, Udriştioiu EG, Aboul-Enein HY (2015) X-ray diffraction: instrumentation and applications. Anal Chem 45:289–299
28. Rhim JW, Hong SI, Park HM, Ng PKW (2006) Preparation and characterization of chitosan-based nanocomposite films with antimicrobial activity. J Agric Food Chem 54:5814–5822
29. Hosseini SF, Zandi M, Rezaei M, Farahmandghavi F (2013) Two-step method for encapsulation of oregano essential oil in chitosan nanoparticles: preparation, characterization and in vitro release study. Carbohydr Polym 95:50–56
30. Ieva E, Trapani A, Cioffi N, Ditaranto N, Monopoli A, Sabbatini L (2009) Analytical characterization of chitosan nanoparticles for peptide drug delivery applications. Anal Bioanal Chem 393:207–215
31. Kalaivani R, Maruthupandy M, Muneeswaran T, Hameedha Beevi A, Anand M, Ramakritinan CM, Kumaraguru AK (2018) ynthesis of chitosan mediated silver nanoparticles (Ag NPs) for potential antimicrobial applications. Front Lab Med 2:30–35
32. Manikandan A, Sathiyabama M (2015) Green synthesis of copper-chitosan nanoparticles and study of its antibacterial activity. J Nanomed Nanotechnol 6:1000251
33. Chae KS, Shin CS, Shin WS (2018) Characteristics of cricket (Gryllus bimaculatus) chitosan and chitosan-based nanoparticles. Food Sci Biotechnol 27:631–639
34. Li LH, Deng JC, Deng HR, Liu ZL, Xin L (2010) Synthesis and characterization of chitosan/ZnO nanoparticle composite membranes. Carbohydr Res 345:994–998
35. Boufi S, Vilar MR, Ferraria AM, Botelho-do-Rego AM (2013) In situ photochemical generation of silver and gold nanoparticles on chitosan. Colloids Surf A: Physicochem Eng Asp 439:151–158
36. Trapani A, Giglio ED, Cafagna D, Denora N, Agrimi G, Cassano T, Gaetani S, Cuomo V, Trapani G (2011) Characterization and evaluation of chitosan nanoparticles for dopamine brain delivery. Int J Pharm 419:296–307
37. Matienzo LJ, Winnacker SK (2002) Dry processes for surface modification of a biopolymer: chitosan. Macromol Mater Eng 287:871–880
38. Zhang S, Xiao Q, Xiao Y, Li Z, Xiong S, Ding F, He J (2022) Chitosan based aerogels with low shrinkage by chemical cross-linking and supramolecular interaction. Gels (Basel, Switzerland) 8:131
39. Huang Z, Li Z, Zheng L, Zhou L, Chai Z, Wang X, Shi W (2017) Interaction mechanism of uranium(VI) with three-dimensional graphene oxide-chitosan composite: insights from batch experiments, IR, XPS, and EXAFS spectroscopy. Chem Eng Sci 328:1066–1074
40. Taketa TB, dos Santos DM, Fiamingo A, Vaz JM, Beppu MM, Campana-Filho SP, Cohen RE, Rubner MF (2018) Investigation of the internal chemical composition of chitosan based LbL films by depth-profiling X-ray Photoelectron Spectroscopy (XPS) analysis. Langmuir 34:1429–1440
41. Rashid S, Shen C, Chen X, Li S, Chen Y, Wen Y, Liu J (2015) Enhanced catalytic ability of chitosan-Cu-Fe bimetal complex for the removal of dyes in aqueous solution. RSC Adv 5:90731–90741
42. Zheng Z, Wei Y, Wang G, Wang A, Gong Y, Zhang X (2009) Surface properties of chitosan films modified with polycations and their effects on the behavior of PC12 cells. J Bioact Compat Polym 24:63–82
43. Daniyal W, Fen YW, Saleviter S, Chanlek N, Nakajima H, Abdullah J, Yusof NA (2021) X-ray photoelectron spectroscopy analysis of chitosan-graphene oxide-based composite thin films for potential optical sensing applications. Polymers 13:478

44. Vale MGR, Oleszczuk N (2006) Current status of direct solid sampling for electrothermal atomic absorption spectrometry—a critical review of the development between 1995 and 2005. Appl Spectrosc Rev 41:377–400
45. Ozbeka N, Baysal A (2017) Determination of sulfur by high-resolution continuum source atomic absorption spectrometry: review of studies over the last 10 years. TrAC—Trends Anal Chem 88:62–76
46. Cal-Prieto MJ, Felipe-Sotelo M, Carlosena A, Andrade JM, Lo´pez-Mahı´a P, Muniategui S, Prada D (2002) Slurry sampling for direct analysis of solid materials by electrothermal atomic absorption spectrometry (ETAAS). A literature review from 1990 to 2000 Talanta 56:1–51
47. Rubio R, Sahuquillo A, Rauret G, Quevauviller P (1992) Determination of chromium in environmental and biological samples by atomic absorption spectroscopy: a review. Int J Environ Anal Chem 47:99–128
48. Lagalante AF (1999) Atomic absorption spectroscopy: a tutorial review. Appl Spectrosc Rev 34:173–189
49. Butcher DJ (2005) Atomic absorption spectrometry; interferences and background correction. In: Worsfold P, Townshend A, Poole C (eds) Encyclopedia of analytical science, 2nd edn. Elsevier, pp 157–163
50. Maruca R, Suder BJ, Wightman JP (1982) Interaction of heavy metals with chitin and chitosan. III. Chromium. J Appl Polym Sci 27:4827–4837
51. Azarova YA, Pestov AV, Ustinov AY, Bratskaya SY (2015) Application of chitosan and its N-heterocyclic derivatives for preconcentration of noble metal ions and their determination using atomic absorption spectrometry. Carbohydr Polym 134:680–686
52. Liu XD, Tokura S, Haruki M, Nishi N, Sakairi N (2002) Surface modification of nonporous glass beads with chitosan and their adsorption property for transition metal ions. Carbohydr Polym 49:103–108
53. Wilschefski SC, Baxter MR (2019) Inductively coupled plasma mass spectrometry: introduction to analytical aspects. Clin Biochem Rev 40:115–133
54. Galazzi1 RM, Chacón-Madrid K, Freitas DC, da Costa1 LF, Arruda MAZ (2020) Inductively coupled plasma mass spectrometry based platforms for studies involving nanoparticle effects in biological samples. Rapid Commun Mass Spectrom 34:e8726
55. Geertsen V, Barruet E, Gobeaux F, Lacour J, Taché O (2018) Contribution to accurate spherical gold nanoparticle size determination by single-particle inductively coupled mass spectrometry: a comparison with small-angle X-ray scattering. Anal Chem 90:9742–9750
56. Palomo-Siguero M, López-Heras MI, Cámaraa C, Madrid Y (2015) Accumulation and biotransformation of chitosan-modified selenium nanoparticles in exposed radish (*Raphanus sativus*). J Anal At Spectrom 30:1237–1244
57. Cui C, He M, Chen B, Hu B (2014) Chitosan modified magnetic nanoparticles based solid phase extraction combined with ICP-OES for the speciation of Cr(III) and Cr(VI). Anal Methods 6:8577–8583
58. Palomo-Siguero M, Vera P, Echegoyen Y, Nerin C, Cámara C, Madrid Y (2017) Asymmetrical flow field-flow fractionation coupled to inductively coupled plasma mass spectrometry for sizing SeNPs for packaging applications. Spectrochim Acta B At Spectrosc 132:19–25
59. Blanco-Andujar C (2014) Ph.D. Thesis, Sodium carbonate mediated synthesis of iron oxide NPs to improve magnetic hyperthermia efficiency and induce apoptosis. University College London. Coates J (2006) Interpretation of infrared spectra, a practical approach. In: Meyers RA (ed) Encyclopedia of analytical chemistry. Wiley
60. Qi L, Xu Z, Jiang X, Hu C, Zou X (2004) Preparation and antibacterial activity of chitosan nanoparticles. Carbohydr Res 339:2693–2700
61. Xu Y, Du Y (2003) Effect of molecular structure of chitosan on protein delivery properties of chitosan nanoparticles. Int J Pharm 250:215–226
62. Tang ESK, Huang M, Lim LY (2003) Ultrasonication of chitosan and chitosan nanoparticles. Int J Pharm 265:103–114
63. Varma R, Vasudevan S (2020) Extraction, characterization, and antimicrobial activity of chitosan from horse mussel modiolus modiolus. ACS Omega 5:20224–20230

64. El-Ahmady El-Naggar N, Saber WIA, Zwei AM, Bashir SI ()2022 An innovative green synthesis approach of chitosan nanoparticles and their inhibitory activity against phytopathogenic Botrytis cinerea on strawberry leaves. Sci Rep 12:3515
65. Mondéjar-López M, Rubio-Moraga A, López-Jimenez AJ, Martínez JCG, Ahrazem O, Gómez-Gómez L, Niza E (2022) Chitosan nanoparticles loaded with garlic essential oil: a new alternative to tebuconazole as seed dressing agent. Carbohydr Polym 277:118815
66. Banerjee T, Mitra S, Singh AK, Sharma RK, Maitra A (2002) Preparation, characterization, and biodistribution of ultrafine chitosan nanoparticles. Int J Pharm 243:93–105
67. Harding SE (1994) Determination of diffusion coefficients of biological macromolecules by dynamic light scattering. In: Jones C, Mulloy B, Thomas AH (eds) Microscopy, optical spectroscopy, and macroscopic techniques. Methods in molecular biology, vol 22. Humana Press. https://doi.org/10.1385/0-89603-232-9:97
68. Stetefeld J, McKenna SA, Patel TR (2016) Dynamic light scattering: a practical guide and applications in biomedical sciences. Biophys Rev 8:409–427
69. Qi L, Xu Z, Jiang X, Hu C, Zou X (2004) Preparation and antibacterial activity of chitosan nanoparticles. Carbohydr Res 16:2693–2700
70. Li G, Jiang Y, Huang K, Ding P, Chen J (2008) Preparation and properties of magnetic Fe_3O_4–chitosan nanoparticles. J Alloys Compd 466:451–456